Microscopic relationship between colloid-colloid interactions and the rheological behaviour of suspensions: a molecular dynamics-stochastic rotation dynamics investigation

Juan D. Olarte-Plata[a] and Fernando Bresme[a]

[a]Department of Chemistry, Imperial College London, SW7 2AZ, London, UK.

ARTICLE HISTORY
Compiled July 19, 2018

ABSTRACT
We investigate the dependence of the shear viscosity of suspensions of spherical colloids as a function of the volume fraction of the suspension, the colloid-colloid interactions and the shear rate. We couple molecular dynamics to describe the motion of the colloids with stochastic rotation dynamics (MD-SRD) for the fluid environment by means of stochastic collisions, in order to incorporate hydrodynamics effects leading to non-newtonian responses. The shear viscosity is computed using non-equilibrium simulations by imposing explicit velocity gradients. The impact of the colloid-colloid interactions is examined by modelling the inter-colloid pair potential with a repulsive power law, that allows interpolating different degrees of colloidal softness. The general rheological behaviour of our suspensions can be described with a Krieger-Dougherty like equation, which must be corrected to account for the variations in the maximum packing fraction and non-equilibrium effects arising from the flux of momentum imposed to the suspension, which appear when varying the softness of the inter-colloidal interactions. We further show evidence for non-newtonian behaviour at high Péclet numbers, characterised both by shear thinning and shear thickening, and thus demonstrate these effects can be successfully captured using MD-SRD methods.

KEYWORDS
Shear viscosity; non-equilibrium molecular dynamics; stochastic rotation dynamics; shear thinning; shear thickening.

1. Introduction

Understanding the relationship between microscopic properties and macroscopic behaviour is one of the main challenges of colloidal science. Of particular interest in industrial applications is the ability to tune transport properties by changing the effective interactions between colloids. This challenge appears in the investigation of calcium carbonate, a widely used mineral in the construction and manufacturing sector. Usually ground to powder and suspended in water, its rheological properties can be tuned by organic additives [1]. In a first approximation, the $CaCO_3$ colloidal particles can be understood as a non rigid sphere with variable softness. The shear viscosity of systems composed of soft bodies has been extensively studied both numerically and

CONTACT Juan D. Olarte-Plata. Email: j.olarte@imperial.ac.uk
CONTACT Fernando Bresme. Email: f.bresme@imperial.ac.uk

theoretically. These studies focused on the dependence of the viscosity on the strain rate and the observation of shear thinning [2, 3], as well as the rationalisation of the shear thinning in terms of the equilibrium structure of the fluid [4]. Additional studies investigated the dependence of the shear viscosity with the thermodynamic state, namely, density and pressure, considering different particle interactions [5]. Hydrodynamic interactions have also been studied using Stokesian dynamics [6], revealing the hydrodynamic origin of shear thickening. It has been shown that SRD successfully models the hydrodynamics of fluids, and therefore it provides a good starting point to investigate non-newtonian behaviour, such as shear thickening, using computer simulations.

Despite these advances, there is a number of outstanding questions that prevent us from describing fully the non-equilibrium response of colloidal suspensions. Some of these questions include: predicting the dependence of the shear viscosity on the shear stress, and interpreting non-newtonian behaviours in terms of inter-colloidal interactions. Hence, to advance in the description of the non-equilibrium response of colloidal suspensions we turn to mesoscopic computer simulations. This approach provides an step to improve existing phenomenological formulations. Stochastic Rotation Dynamics (SRD) has been applied successfully to account for hydrodynamic interactions, in sedimentation processes [7] or the cluster formation and the shear softening of the viscosity in a solution of Al_2O_3 particles [8]. More recently, Laganapan *et al.* used SRD algorithms to compute the shear viscosity of spheres at different Péclet numbers [9]. However, no systematic response of the shear viscosity as a function of the Péclet number was found. We show in our work that such non-newtonian response can be reproduced in a range of colloidal suspensions, and tuned by varying the inter-colloidal interactions.

Our paper is structured as follows. Firstly we explain the non-equilibrium MD-SRD algorithm employed here as well as the different inter-colloidal interactions considered in our work. A discussion of our main results on the dependence of the shear viscosity on volume fraction and shear rate follows. Our results section includes a test of the Krieger-Dougherty equation, and we propose a correction to the original equation to take into account the dependence of the relative viscosity with inter-colloidal interactions and shear rate. We also discuss the possibility of using MD-SRD to recover the non-newtonian response reported in experimental studies. We close the article with a summary of our conclusions.

2. Simulation methods

In order to couple the SRD particles and the colloids, we used stochastic collisions, which has been shown to be the most accurate coupling scheme for high packing fractions [10]. We also used the Müller-Plathe algorithm [11], a reverse non-equilibrium method, to investigate the dependence of the shear viscosity on the shear rate.

For the inter-colloid interactions we used a repulsive power-law potential with a generalized exponent, given in Eq. (1):

$$U(r) = \begin{cases} \epsilon \left(\frac{\sigma}{r}\right)^n, & \text{for } r < r_c. \\ 0, & \text{for } r > r_c. \end{cases} \tag{1}$$

where r_{ij} is the inter-particle distance, ϵ is the interaction strength, σ is the particle diameter, $r_c = 2.5\sigma$, is the interaction cutoff and n is an exponent that modifies the softness of the potential. Following previous studies of colloidal suspensions [9, 12], we set the interaction strength to $\epsilon = 2.5k_BT$. Fig. 1 shows the resulting pairwise interaction energies for varying exponents. This model has been investigated before, *e.g.* Hoover *et al.* reported its phase behaviour [13], and more recently, Heyes *et al.* studied the transport properties of fluids modelled with inverse power law interactions, from $n = 4$ up to the hard-sphere limit ($n \to \infty$) [5].

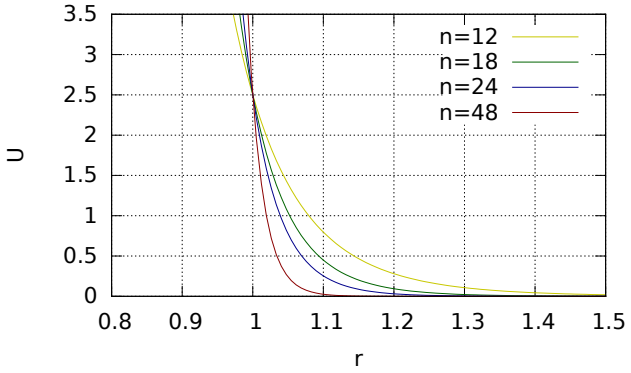

Figure 1. Pairwise interaction energies of colloids with $\epsilon = 2.5$, $\sigma = 1.0$ and different exponents n, according to Eq. 1.

The solvent was modelled with the stochastic rotation dynamics, or multi-particle collision dynamics method, first proposed by Malevanets and Kapral [14]. The SRD algorithm consists of alternating streaming and collisions steps. In the streaming step, particles are streamed for a time-step Δt_{SRD}, and their coordinates are updated with:

$$\mathbf{r}_i(t + \Delta t_{SRD}) = \mathbf{r}_i(t) + \mathbf{v}_i(t)\Delta t_{SRD} \tag{2}$$

After the streaming step, the particles undergo a coarse-grained collision. The simulation box is divided in a regular cubic grid, and within each cell the velocities of the particles are rotated relative to the centre of mass velocity of the cell:

$$\mathbf{v}_i(t + \Delta t_{SRD}) = \mathbf{v}_{cm}(t) + \mathbf{R}_\alpha(\mathbf{v}_i(t) - \mathbf{v}_{cm}(t)) \tag{3}$$

where $\mathbf{v}_{cm}$ is the centre of mass velocity of the particles inside a given cell, and $\mathbf{R}$ is a matrix that rotates the velocity by a fixed angle α around a randomly oriented axis. In this work, we used the LAMMPS implementation of SRD [15], where the rotations are randomly chosen to be around the x, y and z axes, with a fixed rotation angle $\alpha = 90°$.

In order to accurately resolve the hydrodynamics down to the characteristic length scale of the colloidal particles, the grid size for the SRD collision step has routinely been set in the literature to 1/4 of the big particle diameter [16]. We followed the same approach here. With reference to experimental work of calcium carbonate nanoparticles, we choose a colloid diameter of $D = 60$ nm, and set the SRD cell size to $a_0 = 15$ nm. We fixed the number of SRD particles per cell to $\gamma = 5$, following previous works

using SRD [15–17]. It is expected that long ranged hydrodynamic interactions will be appropriately described for colloids located several hydrodynamic radii apart [16]. We choose a mean free path for the SRD particles of $\lambda = 0.6a_0$, which ensures the assumptions of molecular chaos and Galilean invariance [16], since particles can travel to a different SRD cell within collisions. We used a reduced mass density of $\rho_m = 1.0$, therefore, the mass of the SRD particles is $m_{SRD} = 0.25^3$. The SRD time-step is given by $\Delta t_{SRD} = \lambda\sqrt{m_{_{SRD}}/k_BT}$. The reduced temperature in the simulations is $k_BT = 1.0$.

The interaction between an SRD solvent particle and a colloidal particle is modelled through stochastic collisions that impart a force and a torque to the colloid. Rotational degrees of freedom are integrated for the colloidal particles. The collision rule applied here is deemed as a *no-slip* collision, as proposed by Inoue *et al.* [18]. In this collision rule, the new velocity of a colliding SRD particle is assigned as the sum of the local velocity in the collision point $\mathbf{v}_{local}$, and a random velocity with normal and tangential components $\mathbf{v}_n$ and $\mathbf{v}_t$ sampled from the following distributions:

$$p(v_n) \sim v_n exp\left(-\frac{m_{_{SRD}} v_n^2}{2k_BT}\right) \tag{4}$$

$$p(v_t) \sim exp\left(-\frac{m_{_{SRD}} v_t^2}{2k_BT}\right) \tag{5}$$

The local velocity is given by:

$$\mathbf{v}_{local} = \mathbf{v}_{_{colloid}} + \boldsymbol{\omega}_{_{colloid}} \times (\mathbf{r}_i - \mathbf{r}_{_{colloid}}) \tag{6}$$

where $\mathbf{v}_{_{colloid}}$ is the translational velocity of the colloidal particle, $\boldsymbol{\omega}_{_{colloid}}$ is the angular velocity of the colloidal particle, and $\mathbf{r}_i$ and $\mathbf{r}_{_{colloid}}$ are the positions of the SRD and colloidal particles. The tangential component of the random velocity corresponds to a Gaussian distribution at temperature T. The normal component corresponds to a Gaussian distribution at temperature T, restricted to the particles crossing a plane. Since these probability distributions correspond to a thermal equilibrium state of the ideal gas, the collision rules also act as a thermostat on the SRD particles.

The non-equilibrium method for calculating the shear viscosity, introduced by Müller-Plate [11], reverses the traditional view of non-equilibrium approaches. Instead of applying the cause (*i.e.* a shear velocity profile) and observing its effect (the momentum flux or stress), this algorithm imposes a momentum flux via particle swaps, which results in a physical velocity profile. The simulation box is divided in N slabs along the z axis. Particle momentum swaps are performed on the SRD particles only, for slabs at $z = 0$ and $z = L_z/2$, where L is the length of the simulation box. For the slab at $z = 0$, the particle with the most negative momentum in the x direction is selected, while for the slab at $z = L_z/2$ it is the particle with the most positive momentum in the x direction. The swaps conserve the overall kinetic energy of the system. Before applying the non-equilibrium algorithm, we pre-equilibrate the SRD fluid and the colloidal particles for 10^4 time-steps. Subsequently, we introduced the momentum flux, which generates a linear velocity profile after a period of $\sim 2 \times 10^4$ time-steps. We sampled the momentum flux and the velocity profile for an additional 10^5 time-steps.

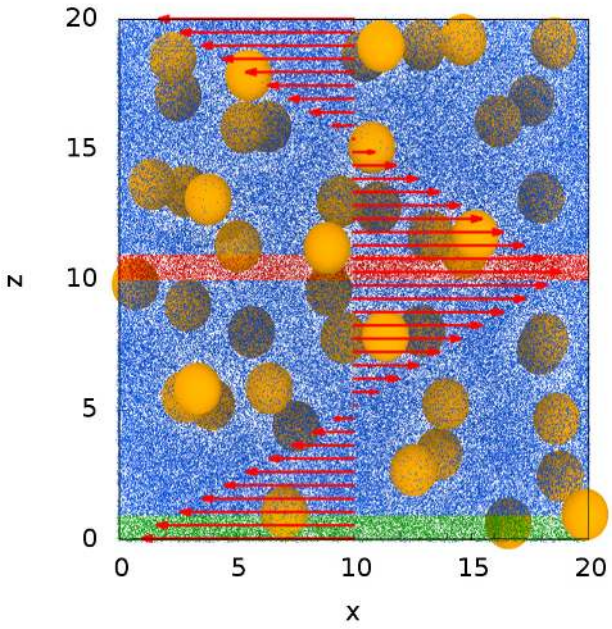

Figure 2. Snapshot of the simulation box showing the colloidal and SRD particles. The two shaded regions highlight the volumes where the SRD particles are selected to perform the Müller-Plathe swaps. We superimpose the resulting linear velocity profile.

At the stationary state, the momentum flux was calculated from:

$$j_z(p_x) = \frac{P_x}{2tA} \tag{7}$$

where P_x is the momentum tally from the swaps performed during a time t, and $A = L_x L_y$ is the cross sectional area of the simulation box. The factor of 2 is included to account for the periodicity of the system (see Fig. 2). The average velocity in the x direction, v_x, is obtained for each of the N slabs of thickness 0.5σ. The gradient of the velocity profile and the momentum flux can be related via:

$$j_z(p_x) = -\eta \frac{\partial v_x}{\partial z} \tag{8}$$

where η is the shear viscosity, which is the key transport property investigated in our work.

3. Results and discussion

We first explore the impact of the simulation cell size on the performance of the non-equilibrium Müller-Plate algorithm, by performing simulations at different swap rates. We have chosen suspensions with a high volume fraction $\phi = 4/3\pi(\sigma/2)^3 N_c/V = 0.40$, where N_c is the number of colloids in a simulation cell with volume V, with box vectors $L_x = L_y = L_z = 5\sigma$, 10σ and 15σ. We analysed simulation conditions using

an equivalent number of swaps for different simulations. This can be achieved by setting $N_{swaps} \propto L^2$, *i.e.* the number of swaps is proportional to the cross-sectional area. We then computed the resulting velocity gradient in the system, as a function of $N_{swaps}/\Delta t_{SRD}/L^2 < 1$. We noticed a dependence of the velocity gradient with the simulation box size, which is connected to the reduction of the fluctuations with increased system size. As a consequence, the maximum velocity gradient achievable decreases with increasing L, as illustrated in Fig. 3a. In all cases, the velocity profiles are found to be linear (Fig. 3b).

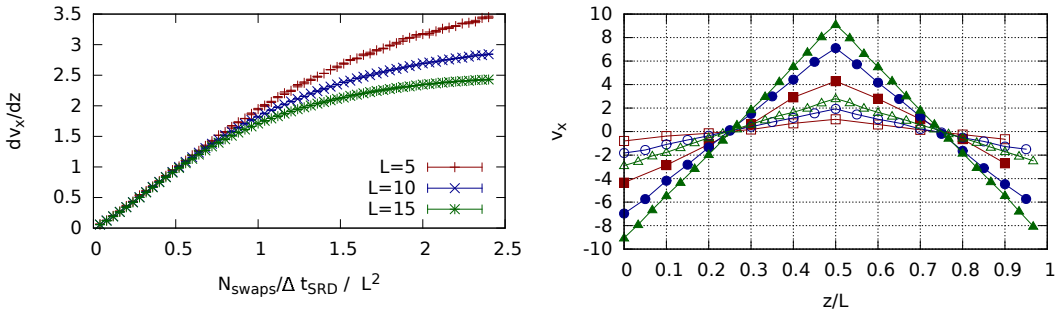

(a) (b)

Figure 3. Left: measured velocity gradient as a function of the number of swaps per SRD time-step, divided by the cross-sectional area of the simulation cell, for a system with $\phi = 0.40$ and different box sizes. Right: velocity profile for L=5 (red), L=10 (blue) and L=15 (green), for $N_{swaps}/\Delta t_{SRD}/L^2 = 0.4$ (open symbols) and $N_{swaps}/\Delta t_{SRD}/L^2 = 2.4$ (closed symbols).

The shear viscosity of the system with a volume fraction $\phi = 0.40$ was computed as a function of the velocity gradient. The interaction exponent was initially set to $n = 48$. We find that the shear viscosity is independent, within the computational accuracy, on system size. Interestingly, the simulations show a clear non-newtonian response in the colloidal suspension, characterised by shear thinning for all the velocity gradients investigated here (see Fig. 4).

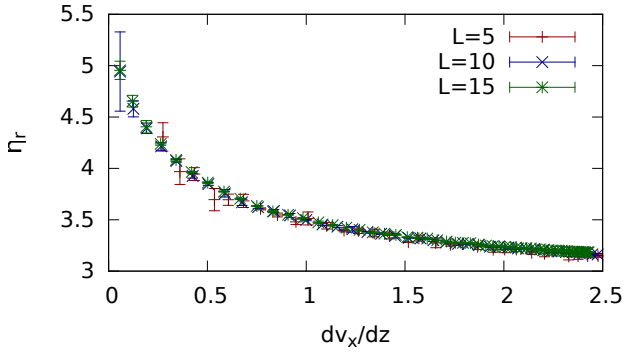

Figure 4. Shear viscosity as a function of the velocity gradient for $\phi = 0.40$ and different box sizes, for a potential with exponent $n = 48$.

3.1. Shear viscosity as a function of the volume fraction

We now explore the variation of the relative shear viscosity of the suspension as a function of the colloidal volume fraction, using different exponents for the inter-colloidal interactions. We have also investigated the role that the momentum flux has on the relative shear viscosity. We show in Fig. 5 the dependence of the relative shear viscosity on the particle softness at fixed values of momentum flux. As expected in colloidal suspensions the viscosity increases with the amount of colloids. In the dilute regime, $\phi < 0.2$, all the suspensions feature the same general dependence of the shear viscosity on the volume fraction. This dependence follows closely the Einstein equation:

$$\eta_r = 1 + 2.5\phi \tag{9}$$

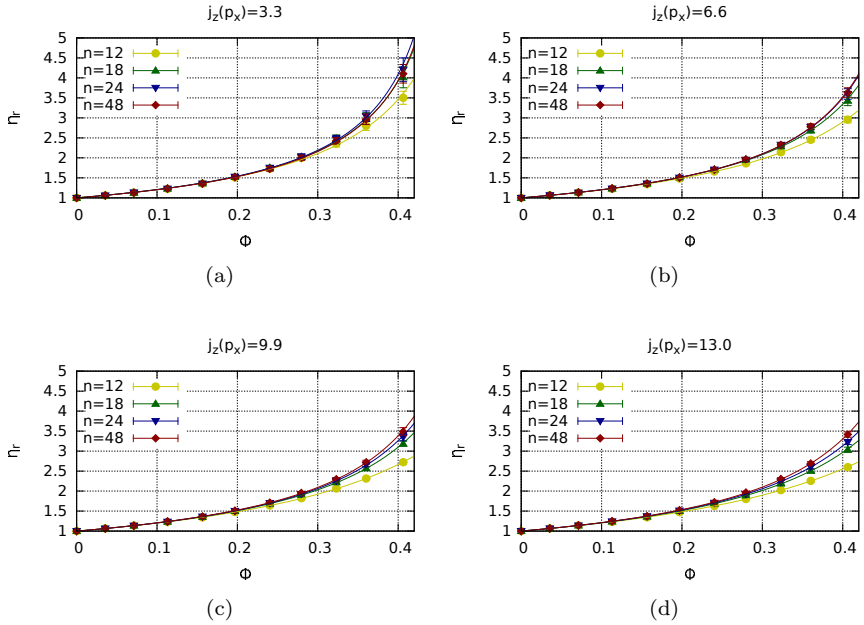

Figure 5. Shear viscosity as a function of the volume fraction and momentum flux for spheres with different exponents n.

where $\eta_r = \eta/\eta_0$ is the relative shear viscosity with respect to the SRD fluid bulk viscosity, η_0. For highly concentrated suspensions, we recover the well known deviation from the linear behaviour (equation (9) of the viscosity with the colloidal volume fraction, with the relative viscosity diverging near the so called "jamming" transition [19]. We used the Krieger-Dougherty (KG) semi-empirical equation [20] to fit relative shear viscosities as a function of volume fraction,

$$\eta_r = \left(1 - \frac{\phi}{\phi_m}\right)^{-p} \tag{10}$$

where ϕ_m is the maximum packing fraction and p is an empirical exponent. Using the KG equation we estimated the exponent p and the maximum packing fraction ϕ_m for

all the cases investigated here. The packing fraction depends strongly on the magnitude of the momentum flux, as well as on the exponent n used to model the inter-colloidal interactions. The dependence is particularly strong for the smallest exponent, 12 (see Fig. 6a).

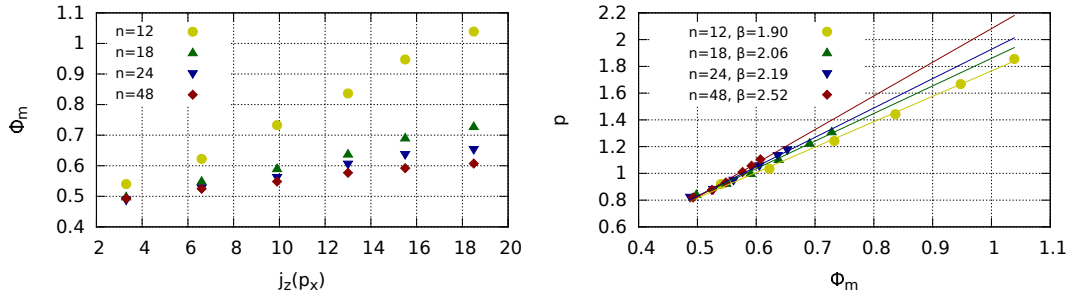

(a) (b)

Figure 6. (Left) Maximum packing fraction ϕ_m as a function of the momentum flux, for exponents $n = 12, 18, 24$ and 48. (Right) Empirical exponent p as a function of the maximum packing fraction ϕ_m, for different particle softness.

For all the interaction exponents investigated here, we find that the maximum packing fraction, ϕ_m, varies linearly with the momentum flux. The differences of ϕ_m become smaller as the momentum flux decreases, and a consistent convergence of $\phi_m \approx 0.5$ is observed for all the colloidal suspensions. These results reveal a clear dependence of the rheological behaviour with the momentum flux which is reflected in deviations of the maximum packing fractions of different colloidal suspensions, which can be explained in terms of the different degree of compressibility of the colloids, and the different exponent determining the inter-colloidal interactions.

We performed additional analyses to determine the relationship between the exponent p and ϕ_m. It has been suggested before that a modified Krieger-Dougherty model can be obtained by introducing a new relation $p = [\eta]\phi_m$, where $[\eta] = \lim_{\phi\to 0}(\eta_r - 1)/(\phi)$ is the so called "intrinsic viscosity", which is a measure of the colloidal contribution to the viscosity at infinite dilution. The intrinsic viscosity for spherical particles is equal to 2.5, larger than 2.5 for other particle shapes, and can be affected by the shear rate due to particle orientation in the flow field, as discussed by Wildemuth and Williams [21]. In cement-water suspensions, it has been reported as varying between 5.1 and 6.8 due to crowding effects [22]. We show in Fig. 6b the dependence of p with ϕ_m, which in our case follows a linear dependence, which can be fitted to $p = \beta\phi_m + c$, hence introducing an extra parameter with respect to previous formulations. The slope β depends on the softness of the potential attaining a value of $\sim$2.5 for the interaction exponent $n = 48$. This value is close to the intrinsic viscosity $[\eta]$ of hard spheres.

To understand the difference in rheological response observed in the suspensions we analysed the colloidal correlations by computing the colloid-colloid radial distribution functions for two different values of Péclet (Pe) number, $Pe = \dfrac{6\pi\eta_0 r^3}{k_B T}\dfrac{\partial v_z}{\partial z} = 0.1$ and 10.

Soft spheres with interaction exponent $n = 12$ feature smaller effective diameters as compared with higher exponents. This effect is particularly evident at the highest Péclet number, 10 (see Fig.8-right), and it is connected to the enhanced interpenetra-

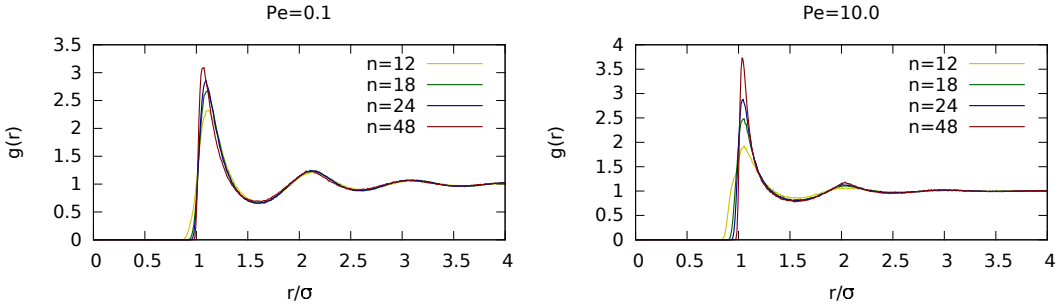

(a) (b)

Figure 7. Radial distribution function for a system with $\phi = 0.40$ and exponents n, for Pe=0.1 (left) and Pe=10 (right).

tion of the particles at high shear rates. The increasing number of overlaps between the colloids at higher concentrations reduces the effective volume fraction of the system. This explains explains the larger ϕ_m we have found (see Fig. 7) and the strong reduction of the shear viscosity at $n = 12$, as compared with larger exponents.

To explore the structural changes induced by shear on the suspensions we computed the two-dimensional radial distribution function (2D-RDF) around a colloid located at $z = L/8$ (see Fig. 2). We chose this location since it is far from the region where momentum swaps are made, and also it has an intermediate value of shear velocity (see Fig. 2). The colloids considered for the construction of the 2D-RDF are those located in a region within a colloidal particle diameter from $z = L/8 = 2.5$. We find strong changes in the microstructure of the suspension. At Pe=1, the radial distribution function around the colloidal particle features weak asymmetries, indicating a prevalence of Brownian motion in the suspension (see Fig.9-left). However, at Pe=10, we observe a strong break of symmetry along the x axis. The asymmetry in the 2D-RDF indicates that the colloids accumulate along the direction of the fluid flow.

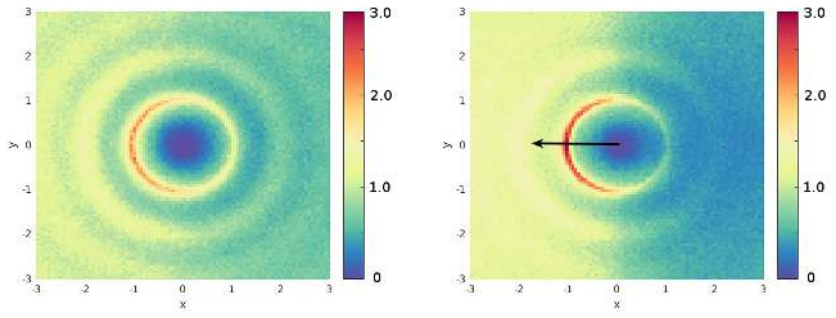

(a) (b)

Figure 8. Two dimensional radial distribution function for a colloidal suspension with $\phi = 0.40$ and Péclet numbers 0.1 (left) and 10 (right). The arrow indicates the direction of the flow. The radial distribution function is built using a 2D histogram, normalized by the number density of the system multiplied by the volume element.

3.2. Shear viscosity as a function of the velocity gradient

In this section we investigate the non-newtonian behaviour of the colloidal suspension as a function of the velocity gradient. These simulations are also used to address the capabilities of the SRD method at high Péclet numbers. We show in Fig. 9 the viscosity as a function of the velocity gradient and the corresponding Péclet number. As noted above the Müller-Plathe algorithm provides an efficient route to set up the fluid flow. However the velocity gradient saturates, hence limiting the range of Péclet numbers that can be achieved using this method. This might restrict the ability of the SRD-non-equilibrium approach to generate states where the hydrodynamic behaviour characteristic of shear thickening dominates. To address this issue we performed additional computations with a suspension with bigger colloids, $\sigma = 2.0$, hence achieving a factor of 8 increase in the Péclet number. Both sets of data $\sigma = 1.0$ and $\sigma = 2.0$ are shown in Fig. 10.

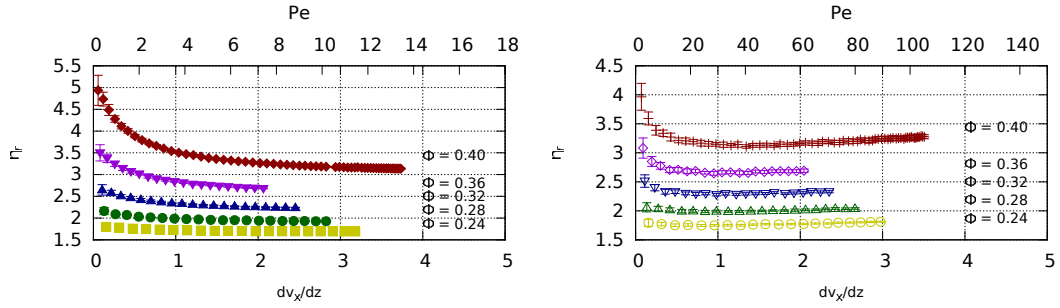

(a) (b)

Figure 9. Shear viscosity as a function of the velocity gradient for a system with $n = 48$, and particle sizes $\sigma = 1.0$ (left) and $\sigma = 2.0$ (right). The different lines represent different volume fractions as indicated in the labels in the corresponding plots.

Unlike in previous works [10], we do find a systematic dependence of the shear viscosity on the velocity gradient. The difference between previous works and our results might be connected to a larger set of Péclet values, as well as more statistical sampling. The shear thinning is increasingly important as the volume fraction is increased, however, it is still noticeable at $\phi \sim 0.25$. For larger Péclet values, achieved by increasing the colloid size, we observe a slight increase in the shear viscosity. This result agrees with previous experimental and numerical results [23] that reported the onset of shear thickening at Péclet values between 10 and 100, depending on the volume fraction of the suspension. To draw a consistent comparison, we rescale the velocity gradient for both colloid sizes with $\sigma = 1$ and $\sigma = 2$ to represent the shear viscosity as a function of the Péclet number.

The shear thinning behaviour is consistent for both particle sizes (see Fig. 10), albeit with some small differences that we attribute to size effects connected to a difference in the ratio between the SRD grid and colloidal particle size.

4. Conclusions

We have shown that the coupling scheme between SRD and MD, along with the reverse non-equilibrium Müller-Plathe algorithm can be used to compute the viscosity of col-

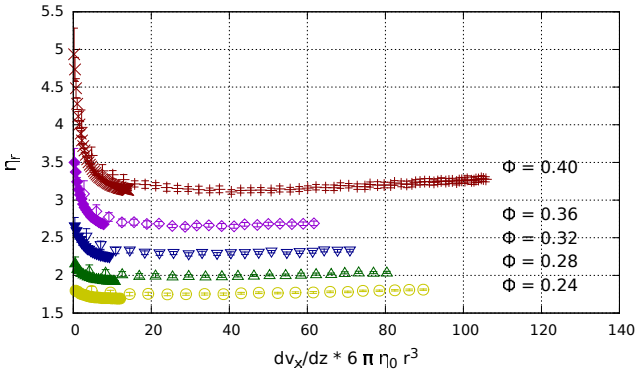

Figure 10. Shear viscosity as a function of the Péclet number for systems with $\sigma = 1.0$ (closed symbols) and $\sigma = 2.0$ (open symbols).

loidal suspensions of spherical colloids, covering a wide range of regimes: from motion dominated by Brownian dynamics to shear thickening observed in the hydrodynamic regime. We further investigated the impact that the inter-colloloidal interactions have on the observed rheological behaviour. We considered different interactions by using a repulsive pair potential with a varying exponent, which allowed us to model colloids with different range of softness. For lower exponents, $n = 12$ the colloids penetrate each other more, while for larger exponents $n = 48$ the colloids approach the hard-sphere behaviour.

We found that at low concentrations, the relative viscosity of the suspension with colloid volume fraction depends little on the inter-colloid interactions. The relative viscosity can be modelled accurately using the Einstein model, a result that is consistent with previous experimental and numerical studies. However, at high packing fractions the inter-colloidal interactions introduce significant differences between suspensions containing soft or hard colloids. Specifically, the relative viscosity varies with the shear rate. Such shear rate dependent effects have been observed before in latex spheres and in cement pastes, and it is reproduced by our model too. The dependence of the relative shear viscosity with the colloid volume fraction can be modelled using the Krieger-Dougherty equation, $\eta_r = (1 - \phi/\phi_m)^{-p(\phi_m)}$ with an exponent that depends on the maximum volume fraction, ϕ_m. Using the SRD simulations we find that $p(\phi_m)$ follows a linear dependence with ϕ_m, $p(\phi_m) = \beta\phi_m + c$, where c is a constant and β is a parameter that converges towards 2.5 at high inter-colloidal repulsions, $n = 48$, and hence it converges to the value reported before for the intrinsic viscosity of hard spheres.

We have also shown that the SRD-non-equilibrium method allows to cover a wide range of dynamic regimes. From low Pe numbers dominated by Brownian dynamics to shear thickening, where hydrodynamic effects become significant, passing through shear thinning. The reproduction of this complex rheological behaviour expands previous studies of suspensions using SRD, and confirms the ability of the method to describe suspensions realistically.

Overall, our work provides insight to advance in the objective of establishing a connection between the dependence of the relative viscosity with volume fraction, and the characteristic interaction between the colloids, by linking the latter to well defined inter-colloidal pair potentials. Our results also highlight the importance of the inter-colloidal repulsion in determining the rheology of the suspension in different Pe

regimes. Hence, care should be exercised in drawing general conclusions when using SRD with specific inter-colloidal interactions.

Acknowledgement This work has been funded through the NanoHeal consortium, part of the European Union Horizon 2020 research and innovation program, under the Marie Sklodowska-Curie grant agreement No. 642976. We thank the Imperial College Research Computing Service for providing computational resources.

References

[1] T. Liberto, M. Le Merrer, C. Barentin, M. Bellotto and J. Colombani, Soft Matter **13** (10), 2014–2023 (2017).
[2] W. Ashurst and W. Hoover, Physical Review A **11** (2), 658–678 (1975).
[3] D.J. Evans and H.J. Hanley, Physical Review A **20** (4), 1648–1654 (1979).
[4] H.J.M. Hanley, J.C. Rainwater and M.L. Huber, International Journal of Thermophysics **9** (6), 1041–1050 (1988).
[5] D.M. Heyes and a.C. Brańka, Physical chemistry chemical physics : PCCP **10** (27), 4036–44 (2008).
[6] D.R. Foss and J.F. Brady, Journal of Rheology **44** (3), 629 (2000).
[7] M. Hecht, J. Harting, T. Ihle and H.J. Herrmann, Physical Review E - Statistical, Nonlinear, and Soft Matter Physics **72** (1), 1–16 (2005).
[8] H. J. Herrmann, J. Harting, M. Hecht and E. Ben-Naim, Brazilian Journal of Physics **38** (1), 37–42 (2008).
[9] A.M.K. Laganapan, A. Videcoq, M. Bienia, T. Ala-Nissila, D. Bochicchio and R. Ferrando, Journal of Chemical Physics **142** (14) (2015).
[10] M. Cerbelaud, A. Maria Laganapan, T. Ala-Nissila, R. Ferrando and A. Videcoq, Soft Matter **13** (21), 3909–3917 (2017).
[11] F. Müller-Plathe, Physical Review E **59** (5), 4894–4898 (1999).
[12] A. Tomilov, A. Videcoq, T. Chartier, T. Ala-Nissilä and I. Vattulainen, Journal of Chemical Physics **137** (1) (2012).
[13] W.G. Hoover, The Journal of Chemical Physics **56** (5), 2207 (1972).
[14] A. Malevanets and R. Kapral, The Journal of Chemical Physics **110** (17), 8605 (1999).
[15] M.K. Petersen, J.B. Lechman, S.J. Plimpton, G.S. Grest, P.J. In 'T Veld and P.R. Schunk, Journal of Chemical Physics **132** (17) (2010).
[16] J.T. Padding and A.A. Louis, Physical Review E - Statistical, Nonlinear, and Soft Matter Physics **74** (3), 1–31 (2006).
[17] D.S. Bolintineanu, J.B. Lechman, S.J. Plimpton and G.S. Grest, Physical Review E - Statistical, Nonlinear, and Soft Matter Physics **86** (6), 1–15 (2012).
[18] Y. Inoue, Y. Chen and H. Ohashi, Journal of Statistical Physics **107** (1-2), 85–100 (2002).
[19] S.L. Shumway, A.S. Clarke and H. Jo **102** (January), 1796–1805 (1995).
[20] I.M. Krieger and T.J. Dougherty, Transactions of the Society of Rheology **3** (1), 137–152 (1959).
[21] C.R. Wildemuth and M.C. Williams, Rheologica Acta **23** (6), 627–635 (1984).
[22] L. Struble and G.K. Sun, Advanced Cement Based Materials **2** (2), 62–69 (1995).
[23] R. Mari, R. Seto, J.F. Morris and M.M. Denn, Proceedings of the National Academy of Sciences **112** (50), 15326–15330 (2015).